

Article

A Novel Tooth Modification Methodology for Improving the Load-Bearing Capacity of Non-Orthogonal Helical Face Gears

Chao Jia *, Bingquan Li and Junhong Xu

School of Mechanical Engineering and Automation, Fuzhou University, Fuzhou 350108, China

* Correspondence: chaojia@fzu.edu.cn

Abstract: This study proposes a double-crown tooth surface modification technology that improves the load-carrying capacity of non-orthogonal helical tooth surface gears. The tooth modification is determined by a modified rack-cutter, and its feed motion is related to an intentionally designed transmission error. The novelty of the tooth modification design is that the transmission error can be pre-designed. First, changing the tooth profile of the tool enables preliminary modification along the tooth profile direction; second, by modifying the interaction between the tool and the machined gear, subsequent fine adjustments are made to the contact path. This two-stage tooth modification strategy not only retains the advantages of the traditional method but also significantly improves the balance of the load distribution on the tooth surface through an original contact path modification strategy. Through systematic tooth contact analysis (TCA) and loaded tooth contact analysis (LTCA), it was verified that the new method reduces contact stress and tooth root bending stress and improves the gear's resistance to misalignment errors. This research provides the basis and motivation for further exploring and improving this tooth profile modification technology to solve the challenges faced by more complex gear systems.

Keywords: non-orthogonal helical face gears; novel tooth modification; tooth contact analysis; loaded tooth contact analysis; load-bearing capacity



Citation: Jia, C.; Li, B.; Xu, J. A Novel Tooth Modification Methodology for Improving the Load-Bearing Capacity of Non-Orthogonal Helical Face Gears. *Machines* **2023**, *11*, 1077. <https://doi.org/10.3390/machines11121077>

Academic Editor: Domenico Mundo

Received: 16 November 2023

Revised: 5 December 2023

Accepted: 6 December 2023

Published: 8 December 2023



Copyright: © 2023 by the authors. Licensee MDPI, Basel, Switzerland. This article is an open access article distributed under the terms and conditions of the Creative Commons Attribution (CC BY) license (<https://creativecommons.org/licenses/by/4.0/>).

1. Introduction

Transmission systems, which are integral to mechanical devices, benefit significantly from the enhancement of gear performance, as it directly affects the overall quality of the equipment. The modification of gear teeth is a prevalent method for enhancing the performance of gear transmission [1–6]. By implementing this technology, the typical line contact found on unmodified gear teeth transitions to point contact after modification. This shift notably diminishes the susceptibility to errors, resulting in a concurrent reduction in both vibration and noise while enhancing the meshing of gears [7]. The process of tooth modification stands out for both its effectiveness and cost-efficiency. It involves precise, micron-level alterations to the gear teeth, leaving the macro structure and overall dimensions of the gear system intact; importantly, it also does not contribute additional weight to the system. Its broad application across diverse gear-driven mechanisms underscores its utility [8–12].

As an evolved transmission variant, face gear systems are pivotal in the realm of machinery, notably within helicopter main reducers, where they have been utilized with considerable success. These systems, due to their rapid operational speeds and substantial load requirements, necessitate tooth modifications [13–17]. The chief aim of teeth modification in this context is to redistribute the forces acting across the teeth surfaces and stabilize the contact patterns in the central tooth zone. Techniques for gear tooth adjustments may include profile, longitudinal, and three-dimensional modifications, collectively referenced here as conventional tooth modification methods. Although these adjustments can lead to diminished vibration and noise, they can inadvertently cause the load to concentrate

in the central region of the teeth, thereby posing a risk for stress concentration. This is particularly concerning in the current landscape where machine loads are progressively increasing, leading to immediate loading of the middle tooth region subsequent to the engagement of the top and root areas. The resulting spike in contact stress can not only accelerate surface wear and reduce the operational lifespan but also decrease the efficiency of gear drives [18–24].

However, there are some limitations in the current tooth surface modification methods, such as the transmission error correction of helical bevel gears and the high-order transmission error (HTE) correction of helical involute gears. These aspects still require further research and improvement. Some researchers have begun to study new methods of tooth surface modification. Su et al. [25] introduced a method to correct transmission errors up to the seventh order in spiral bevel gears. Their research demonstrated that following this correction, the bending stresses on the gear teeth were reduced compared to those observed on parabolic tooth surfaces, with the contact stress remaining largely unaffected. Jiang et al. [26] designed a high-order transmission error correction for helical involute gears through particle swarm optimization (PSO), but there is a lack of correction during the correction process with full consideration of the polynomial coefficients. In addition, Jia et al. [27] proposed a new method based on compensated conjugation to reduce the peak-to-peak transfer error in the design of cylindrical gear tooth surface modification. Yu et al. [28] and Yang et al. [29] proposed an improved tooth surface modification strategy based on spiral theory and the curvature synthesis method. Further research can be carried out on the optimization of transmission performance and surface shape. Mu et al. [30] proposed a functional design-oriented gear design method, emphasizing the importance of gear transmission performance with high-order transmission errors. Samani et al. [31] conducted a nonlinear vibration study on a spiral bevel gear pair with high-order transmission errors and parabolic transmission errors. Korta and Mundo [32] conducted a gear optimization study using the response surface method. Lu et al. [33] developed a tooth profile generation algorithm for non-bevel gears, which is used to correct the pitch points of high-order Archimedes spiral bevel gears and quadratic bevel gears. Finally, Zhao et al. [34] proposed an automatic green onion seedling raising mechanism using an asymmetric transmission high-order non-circular planetary gear train to improve the efficiency of automatic green onion transplanting.

In the above literature, we found that with the continuous improvement of the aviation industry, the new generation of aircraft has put forward higher requirements for face gear transmission systems. Therefore, further research on face gear modification technology still has important practical significance. Traditional modification methods can effectively reduce contact stress, but there is a risk of stress concentration. In order to improve the load-bearing capacity of non-orthogonal helical tooth surface gears, we propose a novel tooth profile modification method, namely the double crown modification method. This method performs corrections along the direction of the tooth profile and the direction of the contact path. By comparing the results of traditional tooth modifications with standard teeth, with and without misalignment errors, the effect of this new tooth modification method is verified.

2. Generation of Non-Orthogonal Helical Face Gear Pair

2.1. Generation of Tooth Surface of Face Gear

As shown in Figure 1, the face gear machining process is carried out by using a grinding wheel to simulate a single-tooth gear cutter. The grinding wheel is regarded as a single tooth of the gear cutter, which moves in the direction of the tooth face while rotating and cutting itself, where S_2 , S_g , and S_5 are rigidly connected to the face gear, the disk grinding wheel and the virtual cutter, and Z_2 , Z_g , and Z_5 are the corresponding rotation axes, respectively.

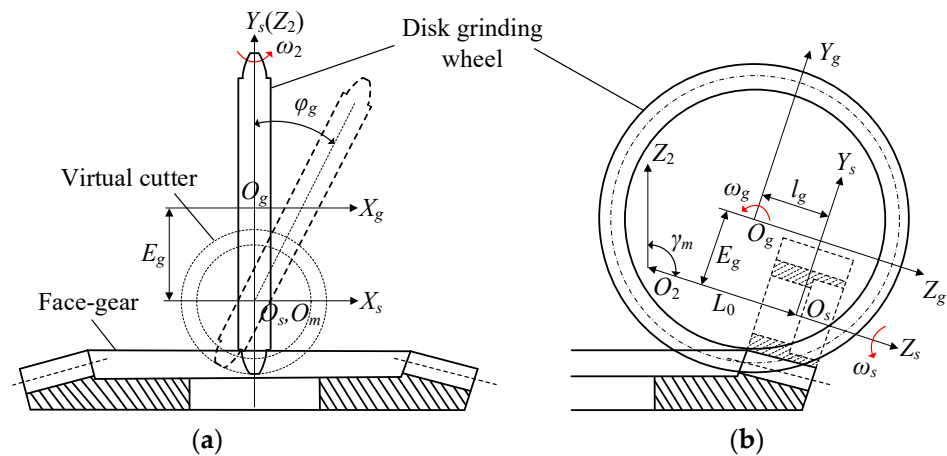


Figure 1. Schematic diagram of face gear machining. (a) Front view; (b) side view.

The distance between the origin O_2 and O_s of the two coordinate systems S_2 and S_5 is L_0 , and the angle γ_m is the shaft angle. The center distance between the disk grinding wheel and the virtual cutter is E_g , and E_g is defined as $E_g = r_g - r_{ps}$, where r_{ps} is the radius of the pitch circle of the virtual cutter, and r_g is the radius of the pitch circle of the disk grinding wheel; l_g is the moving distance of the center of the disk grinding wheel. There are three kinds of motion during the grinding process: the disc-shaped grinding wheel swings around the rotation axis Z_s of the virtual gear shaping cutter at an angular velocity ω_s , the face gear rotates around its own rotation axis Z_2 at an angular velocity ω_2 , and the grinding wheel rotates around its own rotation axis X_g at a high speed ω_g to form a cutting motion.

Through the movement of the tool and the face gear, the position vector of the virtual tool is converted from the coordinate system S_5 to the coordinate system S_2 [35]. Then, the tooth surface of the face gear is generated using the meshing equation.

What is clearly shown in Figure 2 above is a detailed tooth profile illustration of the rack-cutter specifically designed for the purpose of machining the theoretical tooth surfaces of the disk grinding wheel. According to the knowledge of the fundamental principle of gear meshing theory, the tooth surface of the disk grinding wheel depicted in Figure 1 is meticulously shaped through the process of enveloping the toothed surface of the rack-cutter.

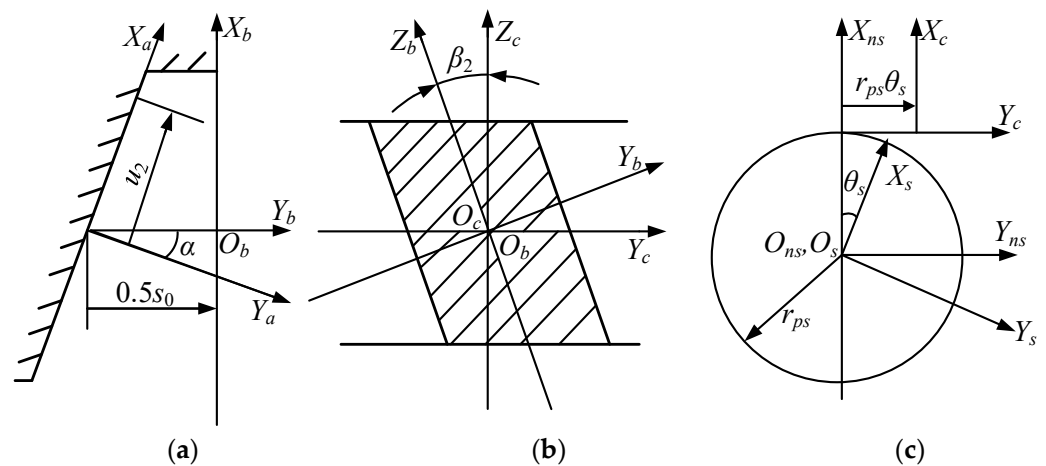


Figure 2. Tooth profile of the rack-cutter. (a) Tooth profile schematic; (b) schematic diagram of helix angle; (c) machining schematic; (where s_0 is the pitch of the round segment; α is the pressure angle of the rack-cutter; β_2 is the helix angle).

The tooth profile of the rack-cutter is determined via Equations (1) and (2).

$$\vec{r}_{a2} = [-a_{c2}u_2^2, u_2, l_g, 1]^T \quad (1)$$

$$\vec{n}_{a2} = \frac{1}{\sqrt{(-2a_{c2}u_2)^2 + 1^2}} \begin{bmatrix} -2a_{c2}u_2 \\ 1 \\ 0 \end{bmatrix} \quad (2)$$

In the context of tooth profile modification for the cutter, a_{c2} represents the modification parameter. The parameters u_2 and l_g are associated with the flank characteristics of the cutting tool.

The profile of the tooth surface for the hypothetical cutter is defined by Equations (3) and (4).

$$\vec{r}_s(u_2, l_g, \theta_s) = M_{sa} \vec{r}_{a2}(u_2, l_g) \quad (3)$$

$$\vec{n}_s(u_2, \theta_s) = L_{sa} \vec{n}_{a2}(u_2) \quad (4)$$

where M_{sa} is a 4×4 coordinate transformation matrix from S_a to S_{si} , and L_{sa} is a 3×3 submatrix of M_{sa} . M_{sa} is determined via Equation (5).

$$M_{sa} = M_{s,ns} M_{ns,c} M_{cb} M_{ba} \quad (5)$$

$$M_{ba} = \begin{bmatrix} \cos \alpha & \sin \alpha & 0 & -0.5s_0 \cos^2 \alpha \\ -\sin \alpha & \cos \alpha & 0 & 0.5s_0 \sin \alpha \cos \alpha \\ 0 & 0 & 1 & 0 \\ 0 & 0 & 0 & 1 \end{bmatrix} \quad (6)$$

$$M_{cb} = \begin{bmatrix} \cos \beta_2 & 0 & \sin \beta_2 & 0 \\ 0 & 1 & 0 & 0 \\ -\sin \beta_2 & 0 & \cos \beta_2 & 0 \\ 0 & 0 & 0 & 1 \end{bmatrix} \quad (7)$$

$$M_{ns,c} = \begin{bmatrix} 1 & 0 & 0 & r_{ps}\theta_s \\ 0 & 1 & 0 & -r_{ps} \\ 0 & 0 & 1 & 0 \\ 0 & 0 & 0 & 1 \end{bmatrix} \quad (8)$$

$$M_{s,ns} = \begin{bmatrix} \cos \theta_s & -\sin \theta_s & 0 & 0 \\ \sin \theta_s & \cos \theta_s & 0 & 0 \\ 0 & 0 & 1 & 0 \\ 0 & 0 & 0 & 1 \end{bmatrix} \quad (9)$$

In Figure 3, the disk grinding wheel rotates around axis X_g at a high speed ω_g to form a cutting motion.

The tooth surface of the disk grinding wheel is determined by Equations (10) and (11).

$$\vec{r}_g(u_2, \theta_g) = M_{gs} \vec{r}_s(u_2) \quad (10)$$

$$\vec{n}_g(u_2, \theta_g) = L_{gs} \vec{n}_s(u_2) \quad (11)$$

where θ_g is the rotation angle of the face gear; M_{gs} is a 4×4 coordinate transformation matrix from S_s to S_g ; and L_{gs} is a 3×3 submatrix of M_{gs} . M_{gs} is determined via Equation (12).

$$M_{gs} = M_{gt} M_{ts} \quad (12)$$

$$M_{ts} = \begin{bmatrix} 1 & 0 & 0 & 0 \\ 0 & 1 & 0 & -E_g \\ 0 & 0 & 1 & 0 \\ 0 & 0 & 0 & 1 \end{bmatrix} \tag{13}$$

$$M_{gt} = \begin{bmatrix} 1 & 0 & 0 & 0 \\ 0 & \cos \theta_g & \sin \theta_g & 0 \\ 0 & -\sin \theta_g & \cos \theta_g & 0 \\ 0 & 0 & 0 & 1 \end{bmatrix} \tag{14}$$

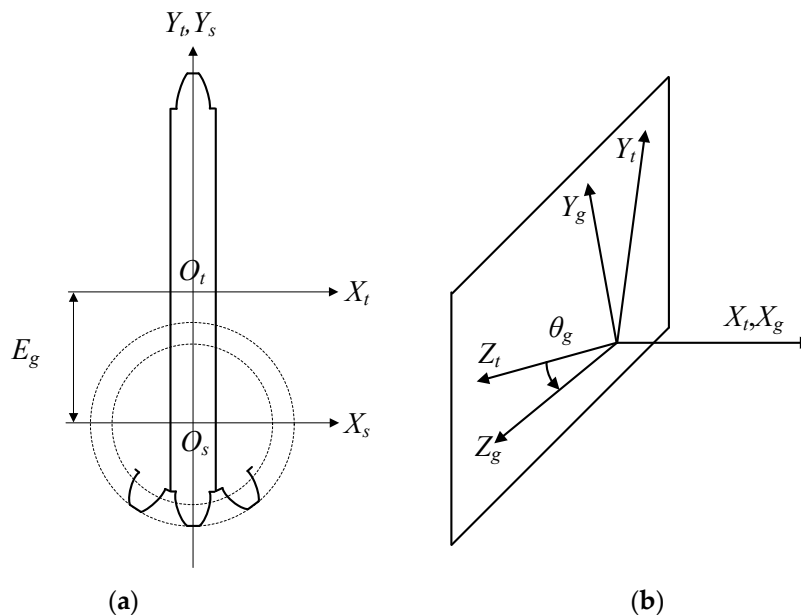


Figure 3. Generation of coordinate system for the disk grinding wheel. (a) Grinding wheel processing; (b) coordinate system machining.

The tooth surface of the face gear is determined by Equation (15).

$$\begin{cases} \vec{r}_2(u_2, l_g, \varphi_g, \theta_g) = M_{2g} \vec{r}_g(u_2, \theta_g) \\ f_1 = \vec{n}_g(u_2, \theta_g) \cdot \vec{v}_{g1}(u_2, l_g, \varphi_g, \theta_g) = 0 \\ f_2 = \vec{n}_g(u_2, \theta_g) \cdot \vec{v}_{g2}(u_2, l_g, \varphi_g, \theta_g) = 0 \end{cases} \tag{15}$$

$$\vec{n}_2(u_2, l_g, \varphi_g, \theta_g) = L_{2g} \vec{n}_g(u_2, \theta_g) \tag{16}$$

where M_{2g} is a 4×4 coordinate transformation matrix from S_g to S_2 , and L_{2g} is a 3×3 submatrix of M_{2g} . f_1, f_2 are the meshing equations of face gears in the coordinate system S_g . \vec{v}_{g1} is the grinding wheel's center speed, while \vec{v}_{g2} is the non-orthogonal helical face gears' relative speed to the grinding wheel. M_{2g} is determined via Equation (17).

$$M_{2g} = M_{2p} M_{ps} M_{sm} M_{mg} \tag{17}$$

$$M_{mg} = \begin{bmatrix} 1 & 0 & 0 & 0 \\ 0 & 1 & 0 & E_g \\ 0 & 0 & 1 & l_g \\ 0 & 0 & 0 & 1 \end{bmatrix} \tag{18}$$

$$M_{sm} = \begin{bmatrix} \cos \varphi_g & -\sin \varphi_g & 0 & 0 \\ \sin \varphi_g & \cos \varphi_g & 0 & 0 \\ 0 & 0 & 1 & 0 \\ 0 & 0 & 0 & 1 \end{bmatrix} \tag{19}$$

$$M_{ps} = \begin{bmatrix} 1 & 0 & 0 & 0 \\ 0 & \cos \gamma_m & -\sin \gamma_m & -L_0 \sin \gamma_m \\ 0 & \sin \gamma_m & \cos \gamma_m & L_0 \cos \gamma_m \\ 0 & 0 & 0 & 1 \end{bmatrix} \tag{20}$$

$$M_{2p} = \begin{bmatrix} \cos \theta_2 & \sin \theta_2 & 0 & 0 \\ -\sin \theta_2 & \cos \theta_2 & 0 & 0 \\ 0 & 0 & 1 & 0 \\ 0 & 0 & 0 & 1 \end{bmatrix} \tag{21}$$

2.2. Generation of Novel Double-Crowned Tooth Surface of Pinion

This research focuses exclusively on the alteration of the pinion tooth. The innovative tooth modification approach is established through the utilization of a modified rack-cutter, alongside its feeding motion, which correlates with a deliberately engineered higher-order transmission error. By meshing with the modified rack, Figure 4 can clearly see the tooth profile of the pinion before and after modification. The amount of practice in the middle is less, and the amount of shaping in and out is larger.

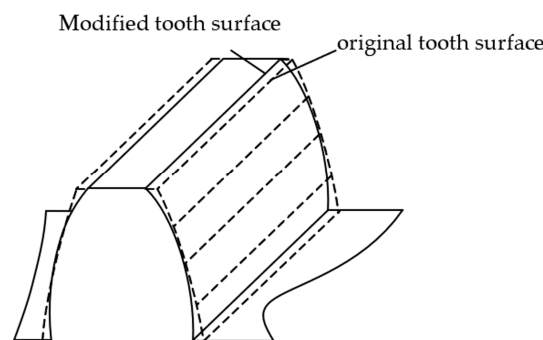


Figure 4. Tooth profile modification renderings.

As shown in Figure 5, the coordinate systems S_{a1} , S_{b1} , and S_{t1} is connected to the rack-cutter. The tooth modification along the tooth profile direction can be realized based on the tooth modification of the rack-cutter.

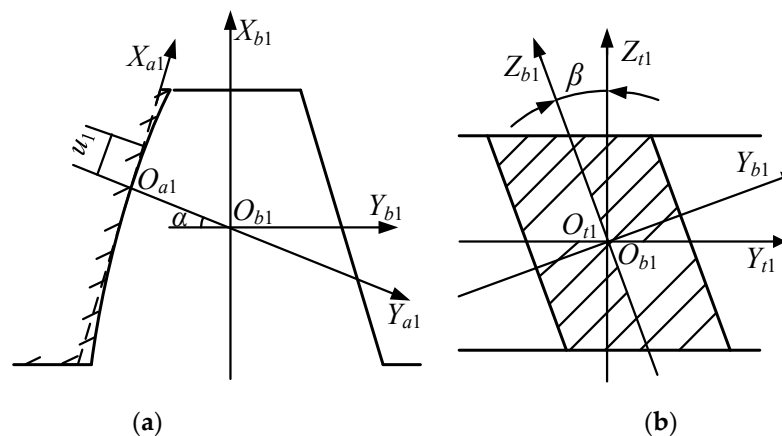


Figure 5. Tooth modification of the rack-cutter of pinion. (a) Second-order parabolic tooth profile; (b) schematic diagram of helix angle.

In Figure 5, the tooth profile of the rack-cutter is a second-order parabola.

As shown in Figure 6, the pinion is generated by the modified rack-cutter. The motion of the rack-cutter and the produced pinion can be changed to achieve a different direction of tooth modification. The produced pinion’s rotating motion is represented by θ_1 . ΔL_1 is the rack-cutter’s extra translation motion parameter, which is related to the intentional designed high-order transmission error. S_{n1} is the fixed coordinate system. r_{p1} is the pitch radius of the pinion. S_{t1} and S_1 are the coordinate systems of the rack-cutter and generated pinion, respectively.

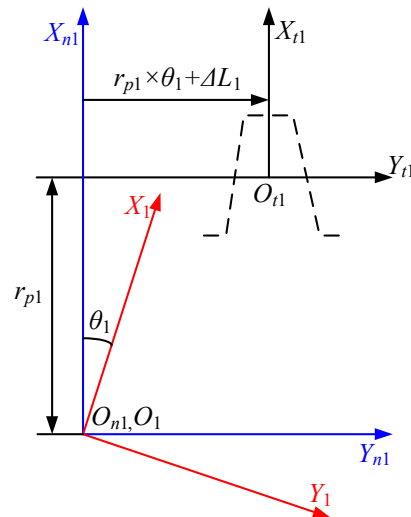


Figure 6. Generation of novel double-crowned tooth surface of pinion.

The double-crowned modified pinion surface can be represented by Equation (22).

$$\begin{cases} \vec{r}_1(u_1, l_1, \Delta L_1, \theta_1) = [M]_{1,t1} \vec{r}_{t1}(u_1, l_1) \\ \vec{n}_1 = [L]_{1,t1} \vec{n}_{t1} \\ f(u_1, l_1, \Delta L_1, \theta_1) = \left(\frac{\partial \vec{r}_1}{\partial u_1} \times \frac{\partial \vec{r}_1}{\partial l_1} \right) \cdot \frac{\partial \vec{r}_1}{\partial \theta_1} = 0 \end{cases} \quad (22)$$

where $[M]_{1,t1}$ is a 4×4 coordinate transformation matrix from S_{t1} to S_1 and $[L]_{1,t1}$ is a 3×3 submatrix of $[M]_{1,t1}$; \vec{r}_{t1} and \vec{n}_{t1} are vectors in the coordinate system S_{t1} , both obtained via Equation (23).

$$\begin{cases} \vec{r}_{t1}(u_1, l_1) = [M]_{t1,a1} [u_1, a_1 u_1^2, l_1, 1]^T \\ \vec{n}_{t1} = \frac{\partial \vec{r}_{t1}}{\partial u_1} \times \frac{\partial \vec{r}_{t1}}{\partial l_1} / \left| \frac{\partial \vec{r}_{t1}}{\partial u_1} \times \frac{\partial \vec{r}_{t1}}{\partial l_1} \right| \end{cases} \quad (23)$$

where a_1 is the modification parameter for the tooth profile modification of the cutter; u_1 and l_1 are the related tooth flank parameters of the cutter.

3. Analysis of Meshing Performance of Face Gears

3.1. Tooth Contact Analysis

The tooth touch analysis (TCA) approach was designed to more effectively assess the real state of the tooth flanks while they are touching, and it is a numerical method to program the mesh process of the tooth flanks $\Sigma 1$ and $\Sigma 2$ with the use of coordinate transformations in order to obtain the contact imprints and the transmission errors. The structure of the face gear sub-structure is shown in Figure 7, with S_1 being the fixed coordinate system of the cylindrical gear and S_2 being the fixed coordinate system of the face gear. In the figure, $B = r_{ps} - r_{p1}$ and $\gamma_f = \gamma_m + \Delta\gamma$, where γ_m is the shaft angle, and $\Delta\gamma$ is the shaft angle error.

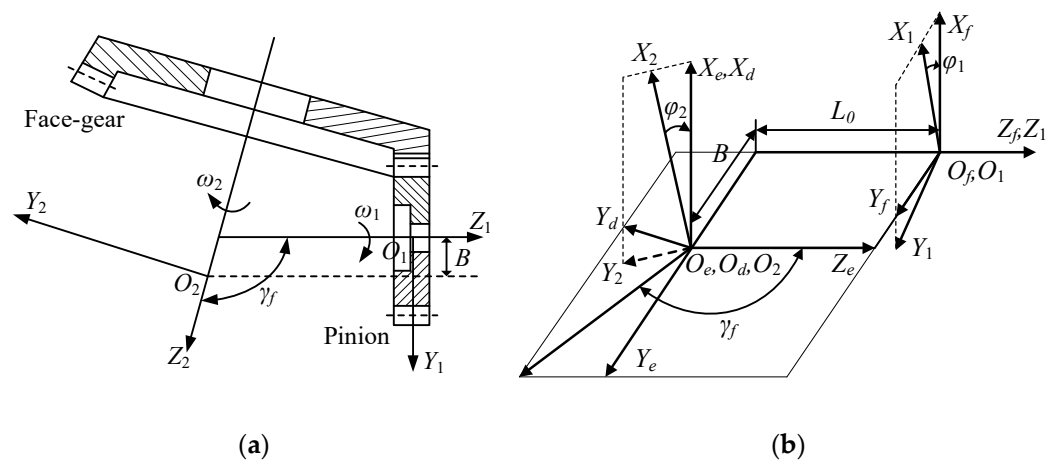


Figure 7. Face gear pair. (a) Face gears; (b) meshing coordinate systems of face gears.

The coordinate transformation method is used to describe the equations for the tooth surface of the pinion and face gears in the coordinate system S_f . Equations (24)–(27) can be used to model the tooth surface.

$$\vec{r}_2^{(f)}(u_2, l_g, \varphi_g, \theta_g, \varphi_2) = M_{f2} \vec{r}_2(u_2, l_g, \varphi_g, \theta_g) \quad (24)$$

$$\vec{r}_1^{(f)}(u_1, l_1, \varphi_1) = M_{f1} \vec{r}_1(u_1, l_1) \quad (25)$$

$$\vec{n}_2^{(f)}(u_2, l_g, \varphi_g, \theta_g, \varphi_2) = L_{f2} \vec{n}_2(u_2, l_g, \varphi_g, \theta_g) \quad (26)$$

$$\vec{n}_1^{(f)}(u_1, l_1, \varphi_1) = L_{f1} \vec{n}_1(u_1, l_1) \quad (27)$$

where $\vec{r}_1^{(f)}$ and $\vec{r}_2^{(f)}$ are position vectors for the pinion's tooth surface Σ_1 and face gear Σ_2 ; $\vec{n}_1^{(f)}$ and $\vec{n}_2^{(f)}$ are unit normal vectors for the pinion's tooth surface $\vec{r}_1^{(f)}$ and the face gear $\vec{r}_2^{(f)}$, respectively; M_{fi} ($i = 1, 2$) is a 4×4 matrix; L_{fi} ($i = 1, 2$) is a 3×3 submatrix of M_{fi} ($i = 1, 2$).

According to the principle of gear meshing, two gears will have a common contact point, which should satisfy that in the same coordinate system, the position vector of this meshing point is the same and the unit normal vector is also the same on both tooth faces. The above conditions can be represented by Equation (28).

$$\begin{cases} f_2(u_2, l_g, \varphi_g, \theta_g) = 0 \\ \vec{r}_2^{(f)}(u_2, l_g, \varphi_g, \theta_g, \varphi_2) = \vec{r}_1^{(f)}(u_1, l_1, \varphi_1) \\ \vec{n}_2^{(f)}(u_2, l_g, \varphi_g, \theta_g, \varphi_2) = \vec{n}_1^{(f)}(u_1, l_1, \varphi_1) \end{cases} \quad (28)$$

where φ_2 is the rotation angle of the face gear; φ_1 is the rotation angle of the pinion.

Considering edge contact, when one of the pinion teeth exits meshing, the contact range is truncated from the original ellipse to a semi-ellipse, which is obviously smaller than the contact area in normal meshing, resulting in stress concentration. Currently, the coordinate system in which the two tooth surfaces are located is S_f , the distance between the tooth contact point and the coordinate origin is the same, and the tangent vector of the pinion's tooth top at the contact point is perpendicular to the normal vector of the tooth surface of the face gear. When the pinion enters into meshing, there is also a truncation of the contact area, resulting in edge contact. By placing the two tooth surfaces in the same coordinate system S_f , the distance from the tooth contact point to the coordinate origin is

the same, and the top edge tangent vector of the face gear is perpendicular to the tooth normal vector of the pinion.

Both cases can be represented by Equations (29) and (30).

$$\frac{\partial \vec{r}_1^{(f)}(u_1, l_1, \varphi_1)}{\partial l_1} \cdot \vec{n}_2^{(f)} = 0 \quad (29)$$

$$\frac{\partial \vec{r}_2^{(f)}(u_2, l_g, \varphi_g, \theta_g, \varphi_2)}{\partial l_g} \cdot \vec{n}_1^{(f)} = 0 \quad (30)$$

where $\frac{\partial \vec{r}_1^{(f)}(u_1, l_1, \varphi_1)}{\partial l_1}$ is the tangent vector of the edge of the crest of the pinion; $\frac{\partial \vec{r}_2^{(f)}(u_2, l_g, \varphi_g, \theta_g, \varphi_2)}{\partial l_g}$ is the tangent vector of the edge of the crest of the face gear; $\vec{n}_1^{(f)}$ is the normal vector of the tooth surface of pinion; $\vec{n}_2^{(f)}$ is the normal vector of the tooth surface of the face gear.

By solving the above equations, the contact point of the face gear can be determined.

3.2. Calculation of Hertzian Contact Stress

According to the theory of contact mechanics, the contact location is deformed by the load, and the contact area expands outward into an ellipse with the contact point as the center. Among these, the ellipse's center experiences the most deformation and contact stress, which gradually diminishes as it moves outward. The curvature of the position of the contact point affects the size of the elliptical contact region, and a corresponding digitizing program can be written to calculate the corresponding curvature.

The two gears in contact are deformed by the normal load and expand into an elliptical contact area at the original contact point O , according to the Hertzian elastic contact theory [36,37]. The contact deformation is shown in Figure 8, where δ_1 and δ_2 are the shape variables of surface 1 and surface 2, respectively.

$$\frac{B}{A} = \frac{(a^2/b^2)E(e) - K(e)}{K(e) - E(e)} \quad (31)$$

$$F_n = \frac{2}{3}p_0\pi ab \quad (32)$$

$$e = \left(1 - \frac{b^2}{a^2}\right)^{1/2} \quad (33)$$

$$\frac{1}{E^*} = \frac{1 - \nu_1^2}{E_1} + \frac{1 - \nu_2^2}{E_2} \quad (34)$$

$$p_0 = \frac{1.5F_n}{\pi ab} \quad (35)$$

where F_n is the contact point's normal load, a is the ellipse's semi-major axis; b is its semi-minor axis; e is the eccentricity of the ellipse, and $K(e)$ and $E(e)$ are the elliptic integrals of the first and second kinds, respectively; p_0 is the maximum contact stress.

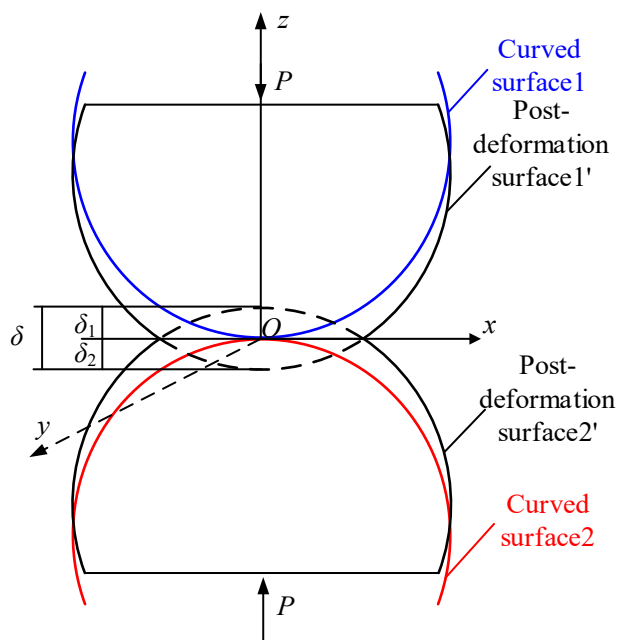


Figure 8. Hertzian elastic contact.

4. Designation of Intentional High-Order Transmission Error

In Figure 9, the transmission error (TE) is pre-designed as a sixth-order parabolic function. The x-coordinate and y-coordinate of the five given points are the rotation angle of the pinion and the transmission error of the face gear, respectively. The points P_A and P_E denote the positions of the gears entering and exiting meshing, respectively. The points P_B and P_D are the two peaks of the curve. The point P_C is the transition point in the middle, and the positional relationship between P_B , P_C , and P_D is determined by the two parameters of λ_B and λ_D . T_m denotes the meshing period of the gears.

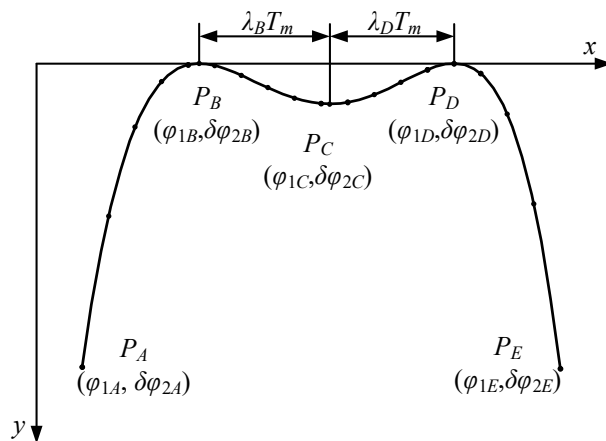


Figure 9. The high-order parabolic transmission error.

The TE function of Figure 8 can be represented as Equation (35).

$$\begin{cases} \delta\varphi_2 = a_0 + a_1\varphi_1 + a_2\varphi_1^2 + a_3\varphi_1^3 + a_4\varphi_1^4 + a_5\varphi_1^5 + a_6\varphi_1^6 = XY^T \\ X = [a_0 \ a_1 \ a_2 \ a_3 \ a_4 \ a_5 \ a_6] \\ Y = [1 \ \varphi_1 \ \varphi_1^2 \ \varphi_1^3 \ \varphi_1^4 \ \varphi_1^5 \ \varphi_1^6] \end{cases} \quad (36)$$

where φ_1 is the rotation angle of the pinion; $\delta\varphi_2$ is the transmission error; $a_0 \sim a_6$ are the coefficients of the HTE function.

Based on the coordinates of the five pre-designed points, the restriction equation of Equation (35) can be written as Equation (36).

$$\begin{cases} x = \varphi_{1A}, & y = \delta\varphi_{2A} \\ x = \varphi_{1B}, & y = \delta\varphi_{2B} \\ x = \varphi_{1B}, & dy/dx = 0 \\ x = \varphi_{1C}, & y = \delta\varphi_{2C} \\ x = \varphi_{1D}, & y = \delta\varphi_{2D} \\ x = \varphi_{1D}, & dy/dx = 0 \\ x = \varphi_{1E}, & y = \delta\varphi_{2E} \end{cases} \quad (37)$$

where

$$\begin{cases} \varphi_{1C} = \frac{\varphi_{1A} + \varphi_{1E}}{2} \\ \varphi_{1B} = \varphi_{1C} - \lambda_B T_m \\ \varphi_{1D} = \varphi_{1C} + \lambda_D T_m \\ T_m = \frac{2\pi}{Z_1} \end{cases} \quad (38)$$

Equation (18) can be written in a matrix form via Equation (38).

$$AX = B \quad (39)$$

where

$$\begin{cases} A = \begin{bmatrix} 1 & \varphi_{1A} & (\varphi_{1A})^2 & (\varphi_{1A})^3 & (\varphi_{1A})^4 & (\varphi_{1A})^5 & (\varphi_{1A})^6 \\ 1 & \varphi_{1B} & (\varphi_{1B})^2 & (\varphi_{1B})^3 & (\varphi_{1B})^4 & (\varphi_{1B})^5 & (\varphi_{1B})^6 \\ 0 & 1 & 2\varphi_{1B} & 3(\varphi_{1B})^2 & 4(\varphi_{1B})^3 & 5(\varphi_{1B})^4 & 6(\varphi_{1B})^5 \\ 1 & \varphi_{1C} & (\varphi_{1C})^2 & (\varphi_{1C})^3 & (\varphi_{1C})^4 & (\varphi_{1C})^5 & (\varphi_{1C})^6 \\ 1 & \varphi_{1D} & (\varphi_{1D})^2 & (\varphi_{1D})^3 & (\varphi_{1D})^4 & (\varphi_{1D})^5 & (\varphi_{1D})^6 \\ 0 & 1 & 2\varphi_{1D} & 3(\varphi_{1D})^2 & 4(\varphi_{1D})^3 & 5(\varphi_{1D})^4 & 6(\varphi_{1D})^5 \\ 1 & \varphi_{1E} & (\varphi_{1E})^2 & (\varphi_{1E})^3 & (\varphi_{1E})^4 & (\varphi_{1E})^5 & (\varphi_{1E})^6 \end{bmatrix} \\ B = [\delta\varphi_{2A} \ \delta\varphi_{2B} \ 0 \ \delta\varphi_{2C} \ \delta\varphi_{2D} \ 0 \ \delta\varphi_{2E}]^T \end{cases} \quad (40)$$

Then, coefficient vector X is calculated via Equation (40).

$$X = A^{-1}B \quad (41)$$

Figure 10 shows the traditional second-order parabolic transmission error. The TE function can be determined by substituting Equation (41) into Equation (40).

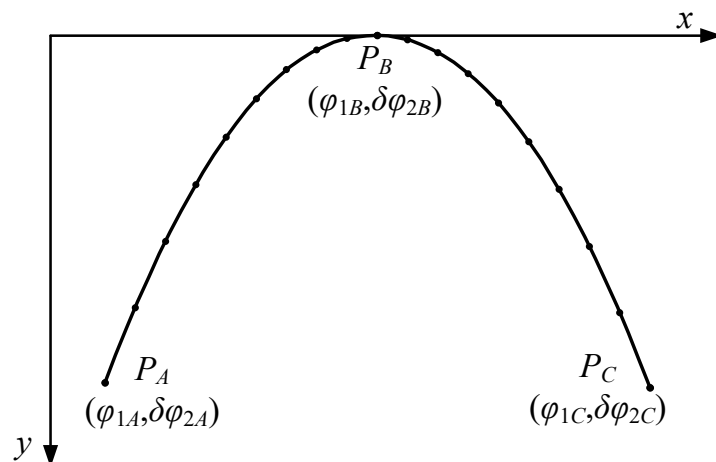


Figure 10. The traditional second-order parabolic transmission error.

$$\left\{ \begin{array}{l} A = \begin{bmatrix} 1 & \varphi_{1A} & (\varphi_{1A})^2 \\ 1 & \varphi_{1B} & (\varphi_{1B})^2 \\ 1 & \varphi_{1C} & (\varphi_{1C})^2 \end{bmatrix} \\ B = [\delta\varphi_{2A} \quad \delta\varphi_{2B} \quad \delta\varphi_{2C}]^T \end{array} \right. \quad (42)$$

where

$$\varphi_{1B} = \frac{\varphi_{1A} + \varphi_{1C}}{2} \quad (43)$$

5. Numerical Examples and Discussions

Only the pinion is modified, herein. The design parameters of the examples of face gears are shown in Table 1. In the following, “non-mod” (non-modification) indicates the results of a tooth surface without modification; “tra-mod” (traditional modification) indicates the results of a tooth surface using the traditional tooth modification method; “nov-mod” (novel tooth modification) indicates the results of a tooth surface using the novel modification method. The input torque was 105 Nm, which was applied to the pinion.

Table 1. Basic design parameters of a non-orthogonal helical face gear.

Parameter	Value
Pinion tooth number	25
Cutter tooth number	28
Face gear tooth number	160
Normal module (mm)	6.35
Pressure angle (degree)	25
Helix angle (degree)	15
Shaft angle (degree)	100
Inner radius (mm)	510
External radius (mm)	600

Figures 11 and 12 shows the face gear tooth and pinion tooth models. Gear tooth face establishment is divided into left tooth face and right tooth face. The gear tooth profile parameters can be substituted into the tooth face equation to obtain the left tooth face, and the rack displacement direction and tooth profile parameters to obtain the opposite number can be processed to obtain the right tooth face of the gear. The steps for generating the tooth surface are as follows:

- (1) Parameter calculation. According to the tooth height of the gear shaping cutter, the tooth height parameter z_2 of the face gear in the coordinate system S_2 is derived;
- (2) Calculate the tooth width. Find the minimum inner diameter R_1 of the gear undercut and the maximum outer diameter R_2 without tooth tip sharpening, and select an appropriate tooth width within the range of R_1 and R_2 as the known quantity y_2 ;
- (3) Discrete y_2 and z_2 . Through discretization, i discrete values of y_{2i} ($y_{21}, y_{22}, y_{23}, \dots, y_{2i}$) and j discrete values of z_{2j} ($z_{21}, z_{22}, z_{23}, \dots, z_{2j}$) are obtained; based on the y_{2i} and z_{2j} , which are used as the input values and substituted into the tooth surface equation, we can obtain $i \times j$ values of θ_{Sij} ($\theta_{Si1}, \theta_{Si2}, \theta_{Si3}, \dots, \theta_{Sij}$) and $i \times j$ values of φ_{Sij} ($\varphi_{Si1}, \varphi_{Si2}, \varphi_{Si3}, \dots, \varphi_{Sij}$);
- (4) Visualization of the working tooth surface. Back-substitute the $i \times j$ group ($\theta_{Sij}, \varphi_{Sij}$) into the non-orthogonal asymmetric surface gear tooth surface equation to obtain $i \times j$ discrete coordinate points (x_{ij}, y_{ij}, z_{ij}) on the corresponding tooth surface, and apply MatLab instructions to generate work surfaces for gears with non-orthogonal faces.

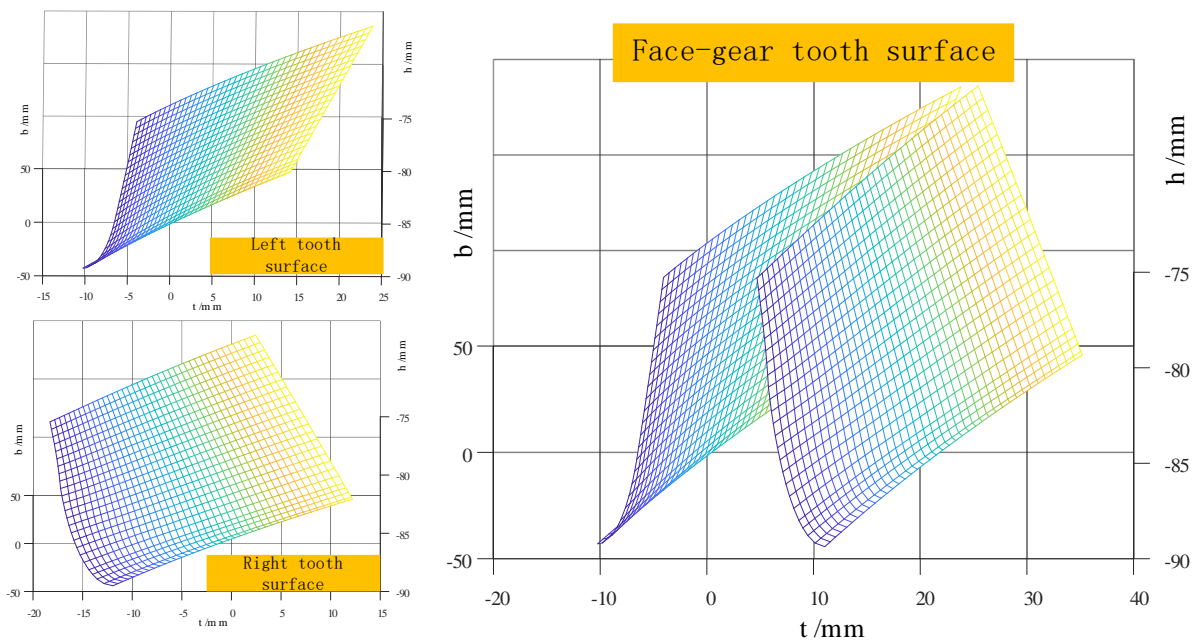


Figure 11. Face gear tooth models.

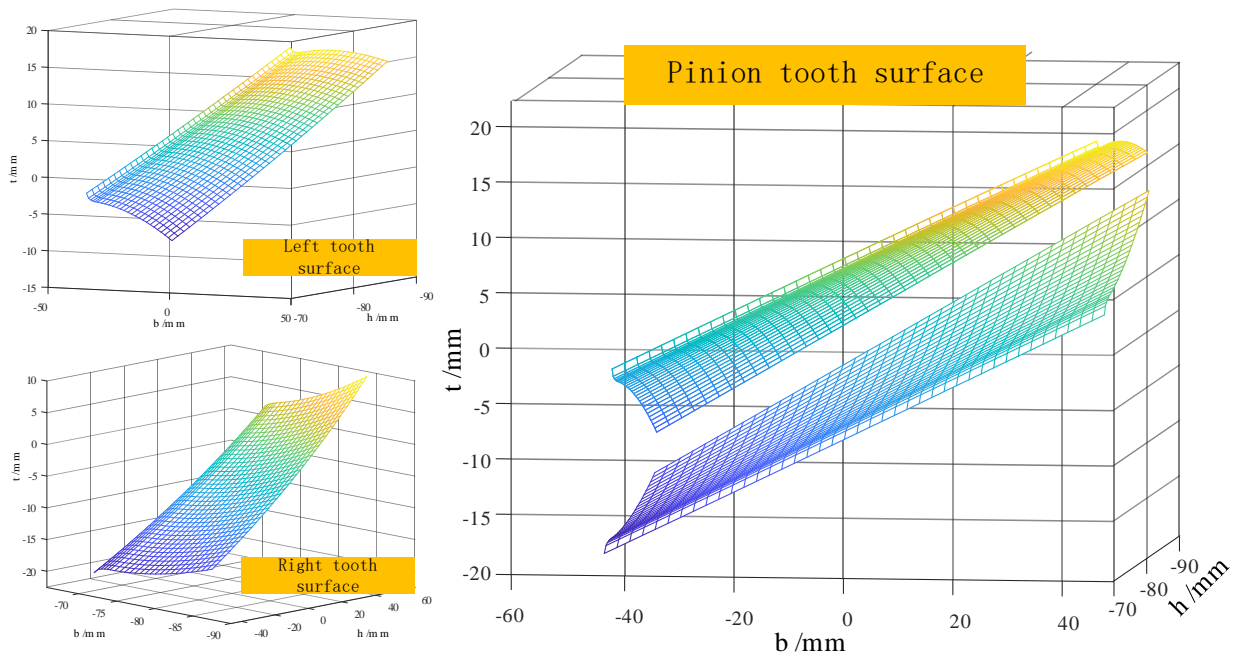


Figure 12. Pinion tooth models.

Similar to the generation method of face gear tooth surfaces, cylindrical gears are also divided into left tooth surfaces and right tooth surfaces. Substitute the tooth shape parameters of the cylindrical gear into the equation, and then use the mesh statement of MATLAB software (2018b) to output the cylindrical gear mesh model, as shown in Figure 12.

5.1. Tooth Modification

Changes in the tooth flanks can often be reflected in the amount of tooth flank modification to study the changes in gear tooth flanks, first analyze the changes in the amount of tooth flank modification.

Figure 13 shows the modification amount of the cylindrical gear tooth surface under different modification methods. As shown in Figure 13a, the cylindrical gear using second-order modification has a medium convex shape, with a small amount of modification in the middle position, and a large amount of modification near the meshing in and meshing out positions. The overall modification amount transitions smoothly, but the uneven distribution of the modification amount on the tooth surface may have adverse effects. In Figure 13b, the cylindrical gear is modified according to the preset HTE. Different from the traditional convex TE, the HTE is concave, and the corresponding tooth surface modification amount is also concave. It can be clearly seen from the modification amount that the high-order modification design ensures a higher modification amount in the middle area, which can make the distribution of the modification amount on the tooth surface more reasonable. At the same time, it ensures that the stress distribution in the middle area of the gear surface is more uniform during meshing, avoiding stress concentration.

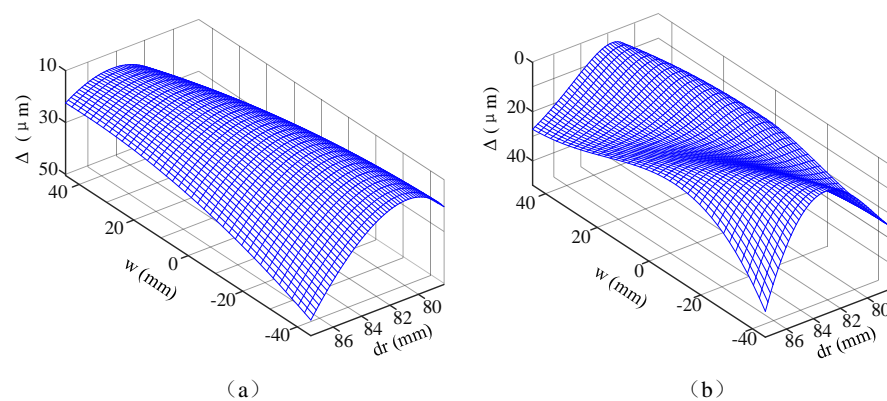


Figure 13. Tooth modification values of the pinion. (a) Tra-mod; (b) nov-mod.

5.2. Tooth Contact Analysis

The contact pattern and the transmission error can be obtained from the TCA calculation. The contact pattern is the main characteristic target of the process of designing, machining, testing, and other related processes due to its intuitiveness, and it is also the key index to measure the transmission and meshing performance of the face gears.

As shown in Figure 14, the TCA calculation results of non-mod, tra-mod, and nov-mod without misalignment error are given. It can be found that the transmission error increases after tooth modification. Furthermore, there are more contact points on the tooth surface, which means that the contact ratio of the face gears increases after the tooth modification. In addition, after tooth modification, the original tooth surface meshing line contact is changed to point contact, so the error sensitivity is reduced. Figure 15 show simplified face gear and pinion transmission models, where Δq is the axial mounting error, ΔE is the offset mounting error, and $\Delta \gamma$ is the misalignment error. The misalignment error has the most significant effect on the face gear TCA results; therefore, this paper focuses on the misalignment error. Figures 16–18 show the variations in the contact pattern and transmission error with the misalignment error for non-mod, tra-mod, and nov-mod, respectively. Compared to the standard installation situation ($\Delta \gamma = 0$), when $\Delta \gamma = 1.5'$, the position of the tooth surface contact point of the face gear continues to shift toward the outer end position, the tooth top edge contact points decrease, the tooth root edge contact points increase, and the meshing position increases. The transmission error also increases significantly. When $\Delta \gamma = -1.5'$, the position of the tooth surface contact point continues to shift toward the inner end position, the tooth root edge contact points decrease, the tooth top edge contact points increase, and the transmission error at the meshing position also increases significantly.

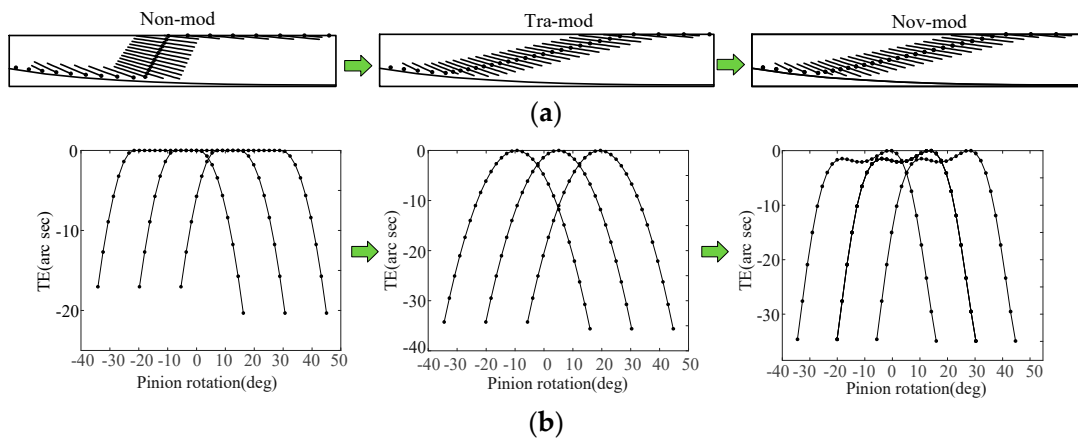


Figure 14. Contact patterns and TEs of non-mod, tra-mod, and nov-mod without misalignment error. (a) Contact patterns; (b) TEs.

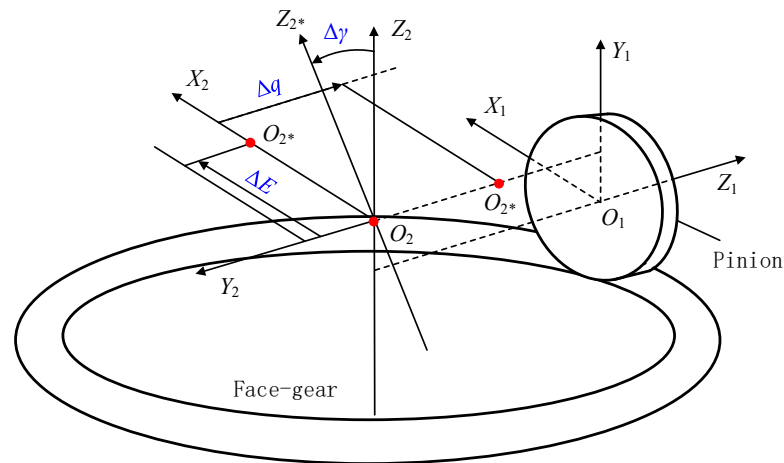


Figure 15. Simplified face gear and pinion transmission models.

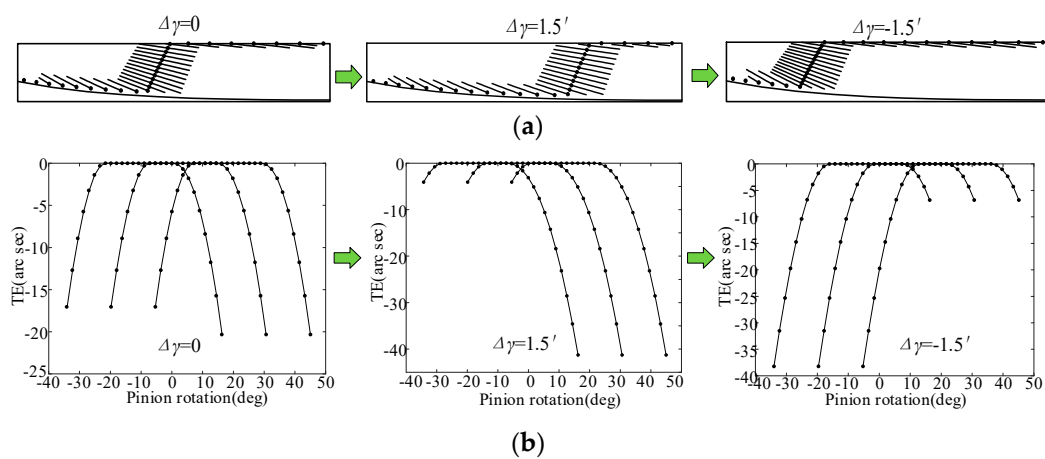


Figure 16. Variations in contact pattern and TE of non-mod with misalignment error. (a) Contact pattern; (b) TEs.

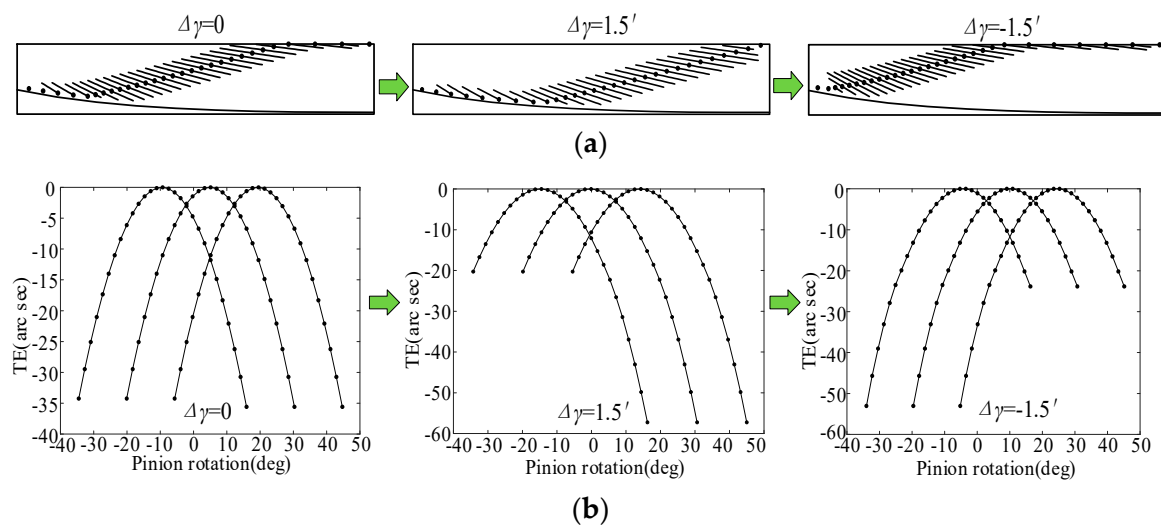


Figure 17. Variations in contact pattern and TE of tra-mod with misalignment error. (a) Contact pattern; (b) TEs.

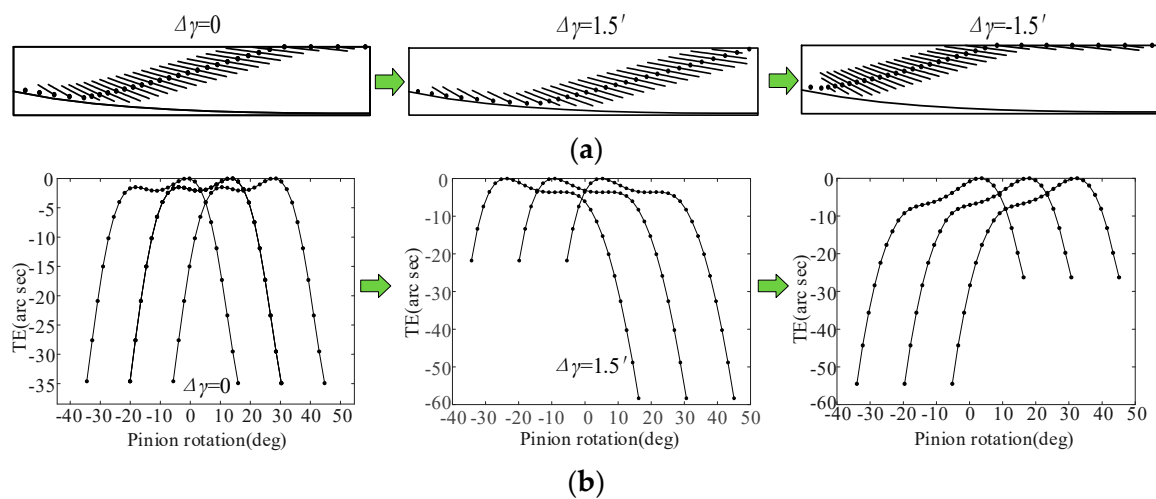


Figure 18. Variations in contact pattern and TE of nov-mod with misalignment error. (a) Contact pattern; (b) TEs.

However, judging from the calculation results of TCA alone, the advantages of the nov-mod are not shown. Therefore, further LTCA of face gears is required to further analyze the loaded meshing performance of the nov-mod.

5.3. Loaded Tooth Contact Analysis

Using ABAQUS software (2021), we conducted a finite element simulation analysis on the non-orthogonal helical tooth surface gear transmission to obtain the contact stress and bending stress when the gear teeth are in contact, thereby judging the performance of the new method of cultivating the subsequent gear transmission. The magnitude of the force applied in this analysis was 1600N·m.

Figure 19 shows the contact stress comparison of non-mod, tra-mod, and nov-mod without misalignment error. Figure 19a–c shows the contact stress nephograms of non-mod, tra-mod, and nov-mod at the position of the pitch circle. It can be seen from the stress nephogram that the contact stress increases after the tooth modification. This is because before tooth modification, the gears are in line contact, but after tooth modification, the gears become point contact, so the contact stress increases. However, it can also be seen that the contact stress of the nov-mod is smaller than that of the tra-mod. This is

because the nov-mod makes the load on the tooth surface more consistent and improves the load distribution.

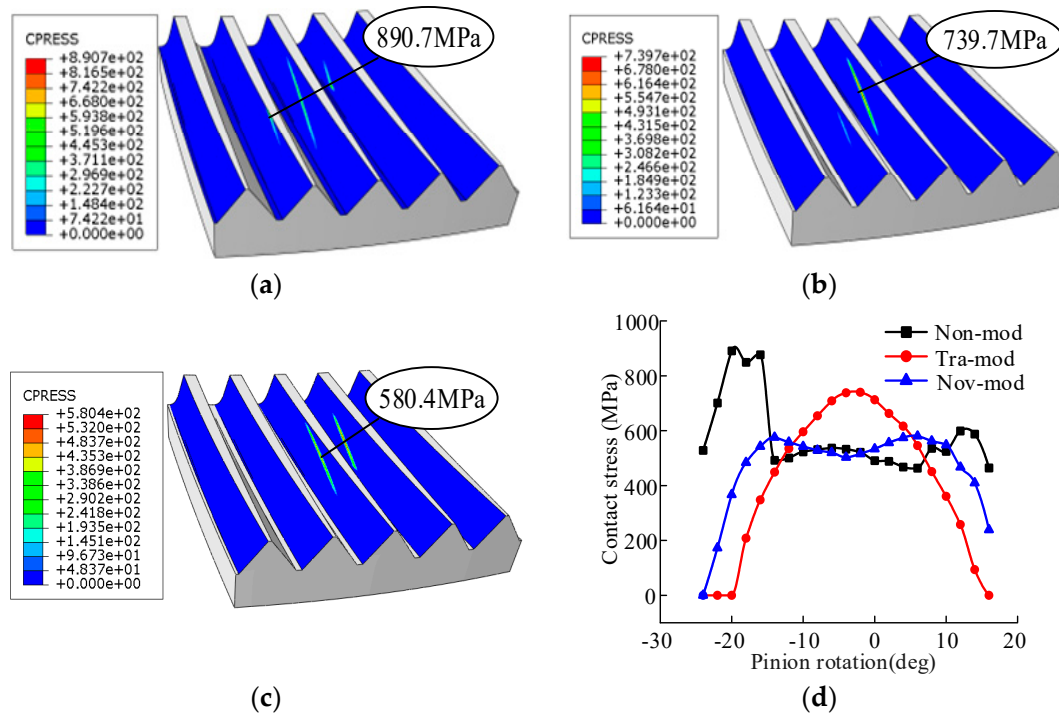


Figure 19. Comparison of the contact stresses without misalignment error. (a) Non-mod; (b) tra-mod; (c) nov-mod; (d) comparison of contact stresses.

Figure 19d shows the contact stress comparison of the three types of tooth surfaces during the whole process from the gear teeth entering the mesh to exiting the mesh. It can be seen from the figure that when entering and exiting the mesh, the contact stress of the non-mod is relatively large because the contact line of the gears is relatively short in these two areas. The maximum contact stress of the non-mod is 890.7 MPa. After tooth modification, the center of the tooth surface experiences an increase in contact stress while the border of the tooth surface experiences a decrease in contact stress. Therefore, tooth modification is beneficial to gear transmission. However, it can also be seen in Figure 19d that the contact stress of the tra-mod in the middle area of the tooth surface increases sharply. The maximum contact stress of the tra-mod is 739.7 MPa. By comparing the contact stress of the nov-mod with that of the tra-mod, the advantages of the nov-mod are shown. The maximum contact stress of the nov-mod is 580.4 MPa. Compared to the tra-mod, the maximum contact stress of the nov-mod is reduced by 34.83%.

Figure 20 illustrates the bending stress comparison of non-mod, tra-mod, and nov-mod without misalignment error. Figure 20a–c shows the bending stress nephograms of non-mod, tra-mod, and nov-mod at the position of the pitch circle. It can be seen in the figures that the tooth modification also has a great influence on the bending stress of the gears. Tooth modification changes the load distribution on the tooth surface and then affects the bending stress of the gears. Figure 20d shows the contact stress comparison of the three types of tooth surfaces during the whole process from the gear teeth entering the mesh to exiting the mesh. In the figure, the maximum bending stresses of the non-mod, tra-mod, and nov-mod are 51.1 MPa, 58.5 MPa, and 44.6 MPa, respectively. Similar to the contact stress, additionally, the nov-mod's bending stress is lower than the tra-mod's, with a decrease of up to 12.72%. The maximum contact stress and maximum bending stress without misalignment errors are shown in Table 2.

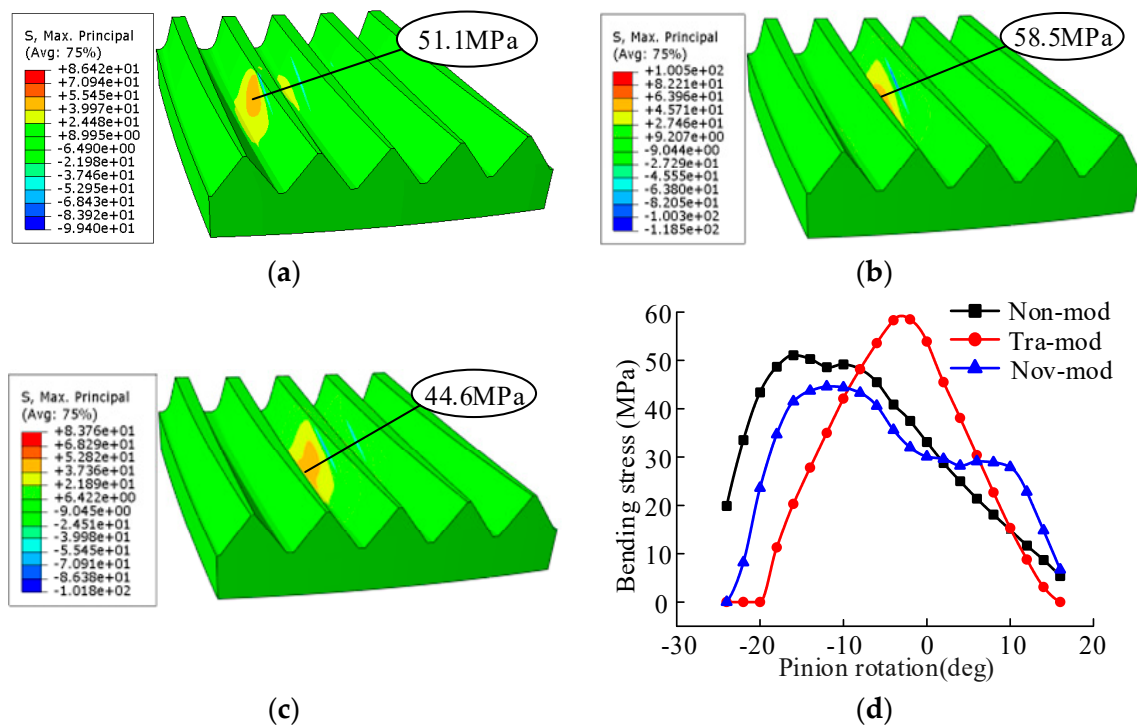


Figure 20. Comparison of the bending stresses without misalignment error. (a) Non-mod; (b) tra-mod; (c) nov-mod; (d) comparison of the bending stresses.

Table 2. Comparison of the maximum contact stress and maximum bending stresses without misalignment error.

Items	Contact Stress		Bending Stress	
	Results (MPa)	Variation	Results (MPa)	Variation
Non-mod	890.7	—	51.1	—
Tra-mod	739.7	−16.95%	58.5	+14.48%
Nov-mod	580.4	−34.83%	44.6	−12.72%

It is well-known that errors in assembly and manufacturing are unavoidable in actual conditions. Therefore, the influence of the misalignment error on the meshing performance of face gears are studied below.

Figure 21 shows the contact stress comparison of non-mod, tra-mod, and nov-mod with misalignment error $\Delta\gamma = 1.5'$. Figure 21d shows the contact stress comparison of the three types of tooth surfaces during the whole process, from the gear teeth entering the mesh to exiting the mesh. The maximum contact stress of non-mod is 858.7 MPa. After tooth modification, the center of the tooth surface experiences an increase in contact stress, while the border of the tooth surface experiences a decrease in contact stress. Therefore, tooth modification is beneficial to gear transmission. However, it can also be seen from Figure 21d that the contact stress of the tra-mod in the middle area of the tooth surface increases sharply. The maximum contact stress of tra-mod is 745.0MPa. By comparing the contact stress of the nov-mod with that of the tra-mod, the advantages of the nov-mod are shown. The maximum contact stress of the nov-mod is 656.2 MPa. Compared to the tra-mod, the maximum contact stress of the nov-mod is reduced by 23.58%.

Figure 22 illustrates the bending stress comparison of non-mod, tra-mod, and nov-mod with misalignment error $\Delta\gamma = 1.5'$. Figure 22d shows the contact stress comparison of the three types of tooth surfaces during the whole process, from the gear teeth entering the mesh to exiting the mesh. In the figure, the maximum bending stresses of non-mod, tra-mod, and nov-mod are 56.4 MPa, 58.5 MPa, and 47.7 MPa, respectively. Similar to the

contact stress, with a decrease of up to 15.42%, the bending stress of the nov-mod is also lower than that of the tra-mod. The maximum contact stress and maximum bending stress with misalignment error $\Delta\gamma = 1.5'$ are shown in Table 3.

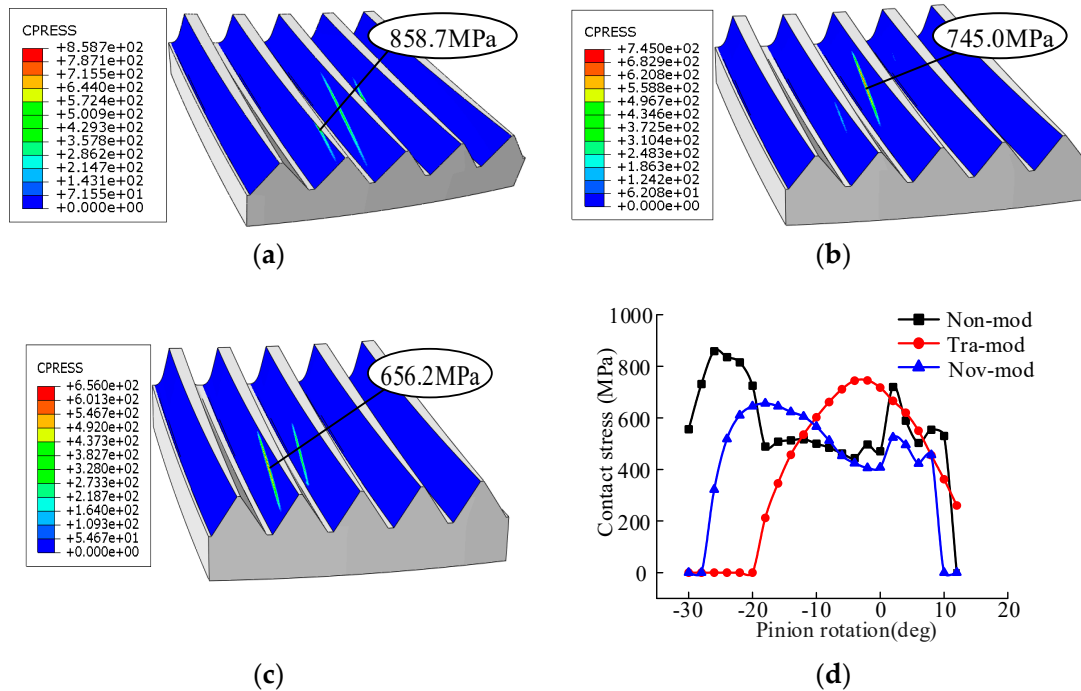


Figure 21. Comparison of the contact stresses with misalignment error, $\Delta\gamma = 1.5'$. (a) Non-mod; (b) tra-mod; (c) nov-mod; (d) comparison of the contact stresses.

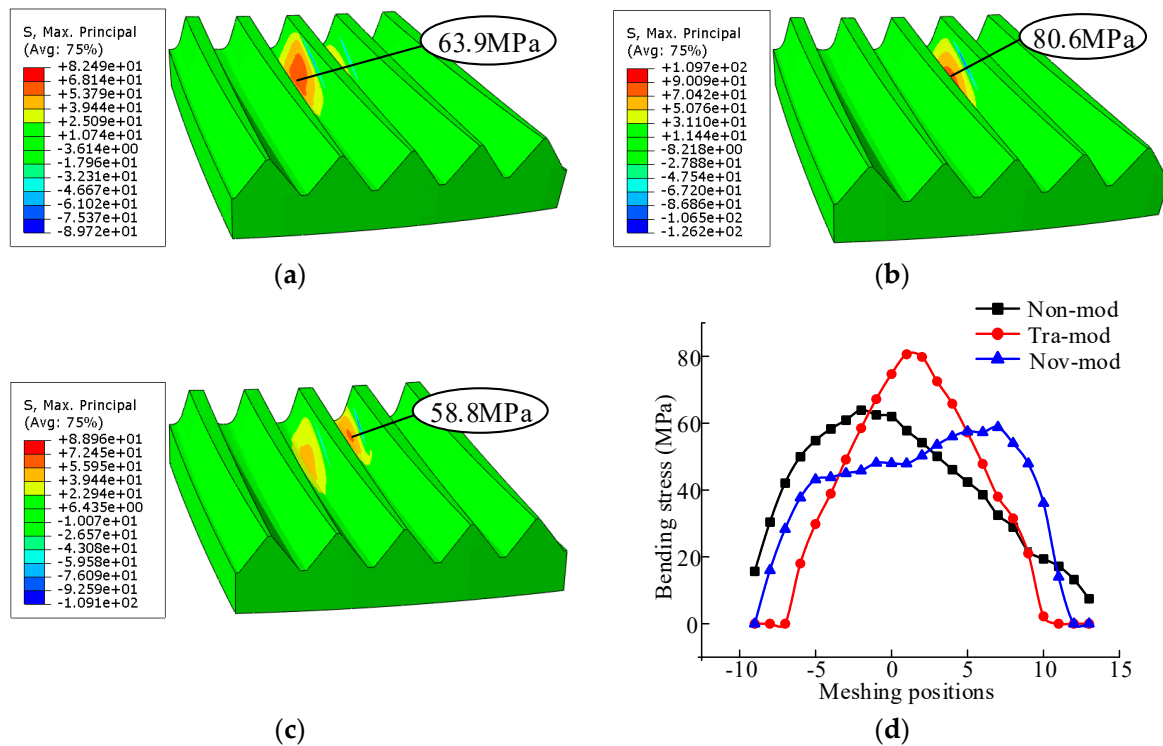


Figure 22. Comparison of the bending stresses with misalignment error, $\Delta\gamma = 1.5'$. (a) Non-mod; (b) tra-mod; (c) nov-mod; (d) comparison of the contact stresses.

Table 3. Comparison of the maximum contact stress and maximum bending stresses with misalignment error, $\Delta\gamma = 1.5'$.

Items	Contact Stress		Bending Stress	
	Results (MPa)	Variation	Results (MPa)	Variation
Non-mod	940.9	—	63.9	—
Tra-mod	774.2	−17.73%	80.6	+26.13%
Nov-mod	694.5	−26.24%	58.8	−7.98%

6. Conclusions

This paper proposes a new gear modification method to improve the load-bearing capacity of non-orthogonal helical gears and draws the following conclusions from the current research:

- (1) This paper proposes a new bidirectional gear modification method. The tooth modification is determined by the modified rack-cutter, and its feed motion is related to an intentionally designed transmission error. The novelty of the tooth modification design is that the transmission error can be predesigned.
- (2) The performance of the introduced novel tooth modification is studied through TCA and LTCA. Under the non-misalignment error working conditions, the contact stress and bending stress of the novel tooth modification decrease by as much as 34.83% and 12.72%, which shows better meshing performance compared to the traditional tooth modification.
- (3) Under the misalignment error working conditions, the contact stress and bending stress of the novel tooth modification decrease by as much as 26.24% and 7.98%. The introduced new gear modification method has lower tooth profile contact stress and tooth root bending stress both with and without misalignment errors.
- (4) The introduced novel tooth modification in this paper is universal, and not limited to face gears but can be extended to other types of gears.

Author Contributions: Conceptualization, C.J.; methodology, C.J.; software, J.X.; validation, B.L.; formal analysis, B.L.; investigation, B.L.; resources, C.J.; data curation, B.L.; writing—original draft preparation, B.L.; writing—review and editing, C.J.; visualization, B.L.; supervision, C.J.; project administration, C.J.; funding acquisition, C.J. and B.L. All authors have read and agreed to the published version of the manuscript.

Funding: The work described in this paper was supported by the National Natural Science Foundation of China (Project Nos. 52375044, 52005107), the Fujian Provincial Science and Technology Major Special Projects (Project No. 2021HZ024006), and the Natural Science Foundation of Fujian Province, China (Project No. 2020J05100).

Institutional Review Board Statement: Not applicable.

Informed Consent Statement: Not applicable.

Data Availability Statement: Data are contained within the article.

Conflicts of Interest: The authors declare that they have no known competing financial interests or personal relationships that could have appeared to influence the work reported in this paper.

Nomenclature

a_1	modification parameter for tooth profile modification
S_i	coordinate system i
u_i, l_i	surface parameter of Σ_i
$[M]_{ij}$	coordinate transmission matrix (from S_j to S_i)
\vec{r}_i, \vec{n}_i	position vector and unit normal vector of surface Σ_i
β	base helix angle

ΔL_1	parameter of additional translation motion of rack-cutter
$\Delta \gamma$	misalignment angle error
$\delta \varphi_2$	transmission error
θ_1	rotation angle of generated pinion
p_0	maximum contact stress
φ_1, φ_2	rotation angle of pinion and face gear
Abbreviations	
Nov-mod	novel modification
Non-mod	non-modification
Tra-mod	traditional modification
TE	transmission error

References

- He, Z.; Lin, H.; Han, X. Computerized design and simulation of meshing of modified double circular-arc helical gears by tooth end relief with helix. *Mech. Mach. Theory* **2010**, *45*, 46–64.
- Chapron, M.; Velex, P.; Bruyère, J.; Becquerelle, S. Optimization of Profile Modifications with Regard to Dynamic Tooth Loads in Single and Double-Helical Planetary Gears with Flexible Ring-Gears. *J. Mech. Des.* **2016**, *138*, 023301. [\[CrossRef\]](#)
- Tran, V.-Q.; Wu, Y.-R. A novel method for closed-loop topology modification of helical gears using internal-meshing gear honing. *Mech. Mach. Theory* **2019**, *145*, 103691. [\[CrossRef\]](#)
- Deng, J.; Nie, S.; Deng, X.; Jiang, C. Tooth surface mismatch modification method of cycloidal bevel gear based on conjugate tooth surface modification. *J. Adv. Mech. Des. Syst. Manuf.* **2020**, *14*, JAMDSM0017. [\[CrossRef\]](#)
- Li, T.; An, X.; Deng, X.; Li, J.; Li, Y. A New Tooth Profile Modification Method of Cycloidal Gears in Precision Reducers for Robots. *Appl. Sci.* **2020**, *10*, 1266. [\[CrossRef\]](#)
- Wang, H.; Tang, L.; Zhou, C.; Shi, Z. Wear life prediction method of crowned double helical gear drive in point contact mixed elas-tohydrodynamic lubrication. *Wear* **2021**, *484*, 204041. [\[CrossRef\]](#)
- Feng, Z.; Chen, Y.; Zhao, Y. Analysis of Influence of Pinion Tooth Trace Modification on Tooth Surface of Curved Tooth Face Gear. *Mech. Transm.* **2022**, *46*, 50–55.
- Huangfu, Y.; Zhao, Z.; Ma, H.; Han, H.; Chen, K. Effects of tooth modifications on the dynamic characteristics of thin-rimmed gears under surface wear. *Mech. Mach. Theory* **2020**, *150*, 103870. [\[CrossRef\]](#)
- Yang, J.; Lin, T.; He, Z.; Chen, M. Novel calculation method for dynamic excitation of modified double-helical gear transmission. *Mech. Mach. Theory* **2022**, *167*, 104467. [\[CrossRef\]](#)
- Ren, Z.Y.; Mao, S.M.; Guo, W.C.; Guo, Z. Tooth modification and dynamic performance of the cycloidal drive. *Mech. Syst. Signal Process.* **2017**, *85*, 857–866. [\[CrossRef\]](#)
- Zschippang, H.; Weikert, S.; Küçük, K.; Wegener, K. Face-gear drive: Geometry generation and tooth contact analysis. *Mech. Mach. Theory* **2019**, *142*, 103576. [\[CrossRef\]](#)
- Dongsheng, H. *Research on Numerical Analysis Modeling Method for Gear Meshing and Its Applications*; Dalian University of Technology: Dalian, China, 2012.
- Yunbo, S. Novel Design Process for Face Gear Drive with a High Order Polynomial Function of Transmission Error. *J. Xi'an Technol. Univ.* **2013**, *33*, 7.
- Li, D.; Wu, S.; Zhao, R.; Deng, X. Design of the high-order curve tooth profile and analysis on the face gear's tooth contact. *Mech. Des.* **2020**, *37*, 109–114.
- Fu, X.; Zhang, Z.; Cui, Y.; Hou, X.; Li, J. Modelling, design and analysis of offset, non-orthogonal and profile-shifted face gear drives. *Adv. Mech. Eng.* **2018**, *10*, 1687814018798250. [\[CrossRef\]](#)
- Fu, X.; Fang, Z.; Xiang, L.; Li, J. Assembly errors tolerance and sensitivity of offset face gears. *J. Harbin Eng. Univ.* **2018**, *39*, 1227–1232.
- Feng, G.; Xie, Z.; Zhou, M. Geometric design and analysis of face-gear drive with involute helical pinion. *Mech. Mach. Theory* **2019**, *134*, 169–196. [\[CrossRef\]](#)
- Wang, C. Multi-objective optimal design of modification for helical gear. *Mech. Syst. Signal Process.* **2021**, *157*, 107762. [\[CrossRef\]](#)
- Gao, P.; Liu, H.; Yan, P.; Xie, Y.; Xiang, C.; Wang, C. Research on application of dynamic optimization modification for an involute spur gear in a fixed-shaft gear transmission system. *Mech. Syst. Signal Process.* **2022**, *181*, 109530. [\[CrossRef\]](#)
- Zheng, F.; Zhang, M.; Zhang, W.; Tan, R.; Guo, X. On the deformed tooth contact analysis for forged bevel gear modification. *Mech. Mach. Theory* **2019**, *135*, 192–207. [\[CrossRef\]](#)
- Yuan, B.; Liu, G.; Yue, Y.; Liu, L.; Shen, Y. A novel tooth surface modification methodology for wide-faced double-helical gear pairs. *Mech. Mach. Theory* **2021**, *160*, 104299. [\[CrossRef\]](#)
- Yan, P.; Liu, H.; Gao, P.; Zhang, X.; Zhan, Z.; Zhang, C. Optimization of distributed axial dynamic modification based on the dynamic characteristics of a helical gear pair and a test verification. *Mech. Mach. Theory* **2021**, *163*, 104371. [\[CrossRef\]](#)
- Yang, Y.C.; Wu, Y.R.; Tsai, T.M. An analytical method to control and predict grinding textures on modified gear tooth flanks in CNC generating gear grinding. *Mech. Mach. Theory* **2022**, *177*, 105023. [\[CrossRef\]](#)

24. Jiang, Y.; Chen, Z.; Tong, S.; Li, S.; Tong, Z. Gear tribodynamic modeling and analysis considering tooth profile modification. *Tribol. Int.* **2023**, *178*, 108023. [[CrossRef](#)]
25. Su, J.; Fang, Z.; Cai, X. Design and analysis of spiral bevel gears with seventh-order function of transmission error. *Chin. J. Aeronaut.* **2013**, *26*, 1310–1316. [[CrossRef](#)]
26. Jiang, J.; Fang, Z. Design and analysis of modified cylindrical gears with a higher-order transmission error. *Mech. Mach. Theory* **2015**, *88*, 141–152. [[CrossRef](#)]
27. Jia, C.; Fang, Z.; Zhang, Y. Topography of modified surfaces based on compensated conjugation for the minimization of transmission errors of cylindrical gears. *Mech. Mach. Theory* **2017**, *116*, 145–161. [[CrossRef](#)]
28. Yu, B.; Ting, K.L. Compensated conjugation and gear tooth design and modification. *J. Mech. Des.* **2016**, *138*, 073301. [[CrossRef](#)]
29. Yang, J.; Shi, Z.; Zhang, H.; Li, T.; Nie, S.; Wei, B. Dynamic analysis of spiral bevel and hypoid gears with high-order transmission errors. *J. Sound Vib.* **2018**, *417*, 149–164. [[CrossRef](#)]
30. Mu, Y.; Li, W.; Fang, Z.; Zhang, X. A novel tooth surface modification method for spiral bevel gears with higher-order transmission error. *Mech. Mach. Theory* **2018**, *126*, 49–60. [[CrossRef](#)]
31. Samani, F.S.; Molaie, M.; Pellicano, F. Nonlinear vibration of the spiral bevel gear with a novel tooth surface modification method. *Meccanica* **2019**, *54*, 1071–1081. [[CrossRef](#)]
32. Korta, J.A.; Mundo, D. Multi-objective microgeometry optimization of gear teeth supported by response surface methodology. *Mech. Mach. Theory* **2017**, *109*, 278–295. [[CrossRef](#)]
33. Lu, G.; Fan, S.; Li, G.; Tong, S.; Xiao, R. Research on Design and Pitch surface shape of New Type High-order Non-conical gears. *Chin. Mech. Eng.* **2015**, *26*, 2989–2995.
34. Zhao, X.; Ye, J.; Chu, M.; Dai, L.; Chen, J. Automatic Scallion Seedling Feeding Mechanism with an Asymmetrical High-order Transmission Gear Train. *Chin. J. Mech. Eng.* **2020**, *33*, 10. [[CrossRef](#)]
35. Litvin, F.L.; Fuentes, A. *Gear Geometry and Applied Theory*; Guo, K., Ye, L., Fan, L., Jr., Eds.; Shanghai Scientific and Technical Publishers: Shanghai, China, 2008; pp. 484–485.
36. Vouaillat, G.; Noyel, J.P.; Ville, F.; Kleber, X.; Rathery, S. From Hertzian contact to spur gears: Analyses of stresses and rolling contact fatigue. *Mech. Ind.* **2019**, *20*, 626. [[CrossRef](#)]
37. Guingand, M.; Vaujany, J.; Jacquin, C.Y. Quasi-static analysis of a face gear under torque. *Comput. Methods Appl. Mech. Eng.* **2005**, *194*, 4301–4318. [[CrossRef](#)]

Disclaimer/Publisher’s Note: The statements, opinions and data contained in all publications are solely those of the individual author(s) and contributor(s) and not of MDPI and/or the editor(s). MDPI and/or the editor(s) disclaim responsibility for any injury to people or property resulting from any ideas, methods, instructions or products referred to in the content.